water

MDPI

Article

Analysis of Tunnel Leakage Hazards and Ecological Environment Response Under Spatial Variability Using Random Fields and PINNs

Buyun Wang [1], Xiaofang Pei [1] and Zhen Liu [2,*]

[1] Anhui Digital Intelligence Construction Research Institute Co., Ltd., Hefei 230088, China
[2] Institute of Space and Earth Information Science, Fok Ying Tung Remote Sensing Science Building, The Chinese University of Hong Kong, Hong Kong SAR, China
* Correspondence: zhenliu@cuhk.edu.hk

Abstract

Tunnel seepage in heterogeneous ground can trigger hydrogeological hazards such as concentrated water inflow, groundwater depletion, deformation of surrounding structures, and subsequent eco-environmental degradation. However, these processes are still commonly evaluated using deterministic models that neglect the spatial variability of hydrogeological parameters. To address this limitation, this study develops a stochastic hydro–geo–mechanical–ecological framework that integrates random field theory with physics-informed neural networks (PINNs) for hazard evaluation and rapid prediction of tunnel seepage responses. The spatial variability of key parameters, including permeability and porosity, is characterized using the Karhunen–Loeve expansion and embedded into coupled governing equations for unsaturated–saturated seepage, seepage–stress interaction, and groundwater–soil–vegetation responses. A PINN surrogate model with random-field inputs is then constructed to predict hydraulic head, tunnel inflow, displacement, groundwater depth, vegetation coverage, and soil physicochemical indices, while simultaneously quantifying uncertainty. A karst tunnel case in Chongqing, China, is used to demonstrate the proposed framework. The results show that spatial heterogeneity promotes preferential flow paths and intensifies seepage-induced hazards compared with deterministic mean simulations, leading to larger groundwater drawdown, stronger ecological degradation, and greater overall response variability. The proposed PINN achieves high predictive accuracy ($R^2 > 0.97$) and reduces single-case computational time from hours to seconds, enabling efficient multi-scenario evaluation and uncertainty-aware risk assessment. This framework provides a physically consistent and computationally efficient tool for evaluating water-related hazards and long-term environmental impacts in underground engineering.

Keywords: tunnel seepage; hydrogeological hazards; random field; physics-informed neural networks; groundwater depletion; uncertainty quantification

Check for updates

Academic Editor: Yeshuang Xu

Received: 24 April 2026
Revised: 2 June 2026
Accepted: 6 June 2026
Published: 10 June 2026

Copyright: © 2026 by the authors. Licensee MDPI, Basel, Switzerland. This article is an open access article distributed under the terms and conditions of the Creative Commons Attribution (CC BY) license.

1. Introduction

With the rapid advancement of transportation infrastructure construction in China, the scale of tunnel engineering under complex geological conditions has been continuously expanding [1]. Particularly in karst-developed regions, high mountainous areas, and ecologically sensitive zones, water seepage induced during tunnel construction and operation has become one of the critical factors restricting engineering safety and ecological

environment protection. Numerous engineering practices demonstrate that tunnel excavation alters the distribution of groundwater dynamic fields and stress fields, frequently triggering a series of cascading ecological responses, including groundwater table decline, surface vegetation degradation, and deterioration of soil physical and chemical properties [2–4]. Therefore, systematically revealing the mechanism of tunnel water seepage and its corresponding geo-ecological environmental responses, as well as establishing efficient prediction methods, possess significant scientific significance and engineering value for ensuring engineering safety and ecological sustainable development.

In recent years, scholars have conducted extensive research on the interaction between tunnel seepage and groundwater systems. Traditional approaches are mostly based on Darcy's law and the continuum assumption, combined with finite-element [5] or finite-difference methods to establish numerical models for simulating groundwater flow and tunnel water inflow processes [6–8]. On this basis, seepage–stress coupling models have been further developed, which can adequately reflect the interaction between surrounding rock deformation and pore water pressure evolution during tunnel excavation [9–11]. Nevertheless, most of the models rely on deterministic parameters and neglect the widespread spatial heterogeneity and randomness in geotechnical media, which are particularly prominent in karst regions, fractured rock masses and sedimentary strata [12–14].

In fact, hydrogeological parameters of rock and soil masses are affected by sedimentary environments, tectonic activities, and weathering processes, exhibiting distinct spatial variability whose statistical characteristics are generally represented as random field distributions [15–17]. In recent years, random field theory has been gradually introduced into geotechnical engineering analysis. Through the K-L expansion or spectral representation method, discretized representation of continuous random fields can be achieved, enabling the incorporation of parameter uncertainty into numerical models [18–20]. Relevant studies indicate that after considering random fields, tunnel water inflow, groundwater drawdown and surrounding rock deformation all present stronger spatial heterogeneity and extreme-value characteristics, while traditional deterministic models tend to underestimate engineering risks [21–23]. Nevertheless, existing studies mostly focus on a single physical field, and systematic research on multi-field coupling interactions and their uncertainty propagation mechanisms remains insufficient.

On the other hand, the impact of tunnel seepage on the ecological environment has attracted increasing attention. Variations in groundwater level directly affect soil moisture content and water supply for vegetation roots, resulting in reduced vegetation coverage and ecosystem degradation [24,25]. Meanwhile, changes in hydrodynamic conditions also influence soil salt migration and nutrient cycling, further exacerbating ecological environment deterioration [26,27]. Most existing studies on ecological responses adopt empirical models or statistical methods, lacking physically coupled descriptions integrated with hydrogeological processes, and thus fail to reveal the multi-field coupling mechanism and its spatial heterogeneity. Therefore, establishing a unified coupled model that simultaneously considers hydrological, mechanical, and ecological responses represents an important developmental trend in current research.

With the development of artificial intelligence, deep learning-based scientific computing methods have gradually emerged as a novel approach to solving complex partial differential equations [28]. Among them, Physics-Informed Neural Networks (PINNs) embed governing equations, boundary conditions, and initial constraints into the loss function, enabling mesh-free solutions to physical processes with the advantages of high efficiency, flexibility, and scalability [29–31]. In recent years, PINNs have been preliminarily applied to groundwater flow, porous media seepage, and consolidation problems, demonstrating favorable accuracy and generalization ability [32–34]. Nevertheless, most existing

PINN studies rely on deterministic parameters, and insufficient consideration has been given to the spatial randomness of geotechnical parameters and the associated uncertainty propagation [35].

Although considerable progress has been made in the study of tunnel seepage, several limitations remain in the existing literature. Most studies are based on deterministic parameter assumptions and therefore cannot adequately capture the influence of spatial variability on seepage behavior. In addition, the coupling between seepage, mechanical response, and ecological effects is often treated separately, lacking an integrated framework. Furthermore, traditional numerical methods are computationally expensive and not well suited for efficient multi-scenario analysis under uncertainty.

To address these limitations, this study integrates random field theory with physics-informed neural networks to establish a coupled hydro–geo–mechanical–ecological model. Compared with previous studies, the proposed approach explicitly incorporates spatial variability, enables efficient prediction through PINN, and provides a unified framework for analyzing multi-field responses and their ecological impacts.

2. Methodology

To clarify the overall structure of the proposed framework, the methodology follows a sequential procedure consistent with the problem formulation presented in the Introduction. First, the spatial variability of hydrogeological parameters is characterized using random field theory and Karhunen–Loève expansion. Second, a multi-field coupled model is established to describe seepage, mechanical response, and ecological processes. Finally, a physics-informed neural network is constructed to efficiently solve the coupled system and quantify the uncertainty of the response fields. Figure 1 presents the overall framework of the proposed methodology.

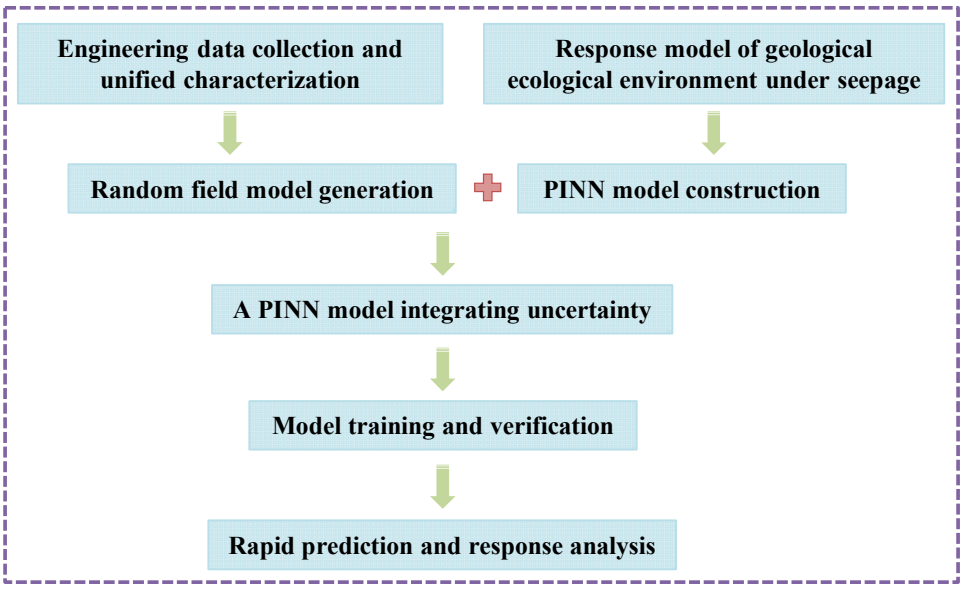


Figure 1. Overall work flow diagram.

2.1. Unified Characterization of Uncertainty in Multi-Source Parameters

2.1.1. Fundamental Theory of Random Fields

The random field $\theta(\mathbf{x}, \omega)$ is defined over the spatial domain $\mathbf{x} \in D \subset \mathbb{R}^d (d = 2, 3)$ and the probability space (Ω, F, P), satisfying the second-order stationarity assumption. Its meaning and covariance function are, respectively [36]:

$$\left.\begin{array}{l} \mu_\theta(\mathbf{x}) = \mathbb{E}[\theta(\mathbf{x}, \omega)] \\ C_\theta(\mathbf{x}, \mathbf{x}') = \mathbb{E}\left[(\theta(\mathbf{x}, \omega) - \mu_\theta(\mathbf{x}))(\theta(\mathbf{x}', \omega) - \mu_\theta(\mathbf{x}'))\right] \end{array}\right\} \quad (1)$$

where $\mathbb{E}[\cdot]$ is the mathematical expectation operator, $\mathbf{x}$ and $\mathbf{x}'$ are spatial coordinates, and $C_\theta(\mathbf{x}, \mathbf{x}')$ is the covariance function of the random field.

The exponential covariance function is adopted to characterize the spatial correlation of geotechnical parameters, and its expression is [37]:

$$C_\theta(\mathbf{x}, \mathbf{x}') = \sigma_\theta^2 \exp\left(-\sum_{i=1}^{d} \frac{|x_i - x_{i'}|}{\theta_{c,i}}\right) \quad (2)$$

where σ_θ^2 is the variance of the random field, and $\theta_{c,i}$ is the correlation length in the i-th spatial direction.

2.1.2. Random Field Discretization Based on K-L Expansion

The K-L expansion decomposes the continuous random field into a sum of products of orthogonal basis functions and independent random variables, and its expression is:

$$\theta(\mathbf{x}, \omega) = \mu_\theta(\mathbf{x}) + \sum_{k=1}^{\infty} \sqrt{\lambda_k} \xi_k(\omega) \varphi_k(\mathbf{x}) \quad (3)$$

where λ_k and $\varphi_k(\mathbf{x})$ are the eigenvalues and eigenfunctions of the covariance operator, respectively, $\xi_k(\omega)$ are independent and identically distributed standard Gaussian random variables, $\mathbb{E}[\xi_k] = 0$, $\mathbb{E}[\xi_k \xi_l] = \delta_{kl}$, and δ_{kl} is the Kronecker delta function.

The eigenvalues and eigenfunctions of the covariance operator satisfy the following integral equation:

$$\int_D C_\theta(\mathbf{x}, \mathbf{x}') \varphi_k(\mathbf{x}') d\mathbf{x}' = \lambda_k \varphi_k(\mathbf{x}) \quad (4)$$

This formula realizes the unified characterization of multi-source parameter uncertainty, transforms the continuous random field into a finite-dimensional random vector $\xi = [\xi_1, \xi_2, \ldots, \xi_M]^T$, and can be efficiently embedded into subsequent coupling models and neural networks.

2.1.3. Coupled Characterization of Multi-Parameter Random Fields

For multi-parameter random fields such as hydraulic conductivity $K(\mathbf{x}, \omega)$ and porosity $n(\mathbf{x}, \omega)$, a joint covariance matrix is constructed:

$$\mathbf{C}(\mathbf{x}, \mathbf{x}') = \begin{bmatrix} C_K(\mathbf{x}, \mathbf{x}') & C_{K,n}(\mathbf{x}, \mathbf{x}') \\ C_{n,K}(\mathbf{x}, \mathbf{x}') & C_n(\mathbf{x}, \mathbf{x}') \end{bmatrix} \quad (5)$$

where $C_{K,n}(\mathbf{x}, \mathbf{x}')$ is the cross-covariance function between parameters, reflecting the correlation of parameter randomness. Through multivariate K-L expansion, the simultaneous discretization of multi-parameter random fields is realized, ensuring the consistency and coupling of the spatial distribution of parameters.

2.2. Theoretical Model of Geo-Ecological Environment Response to Tunnel Seepage

2.2.1. Governing Equation of Unsaturated–Saturated Seepage

Considering the spatial variability of random field parameters, the two-dimensional governing equation of unsaturated–saturated seepage is:

$$S_s(\mathbf{x},\omega)\frac{\partial H}{\partial t}+\frac{\partial}{\partial x_i}\left[K_{ij}(\mathbf{x},\omega,\psi)k_r(\psi)\left(\frac{\partial H}{\partial x_j}-\gamma_{w,j}\right)\right]=Q \tag{6}$$

where H is the total hydraulic head, $S_s(\mathbf{x},\omega)$ is the specific storage of the random field, $K_{ij}(\mathbf{x},\omega,\psi)$ is the permeability tensor of the random field, ψ is the matric suction, $k_r(\psi)$ is the relative permeability, $\gamma_{w,j}$ is the component of gravitational acceleration, Q is the source–sink term, and t is time.

The Van Genuchten model is adopted to describe the soil–water characteristic curve and relative permeability:

$$\left.\begin{aligned}\theta(\psi)&=\theta_r+\frac{\theta_s-\theta_r}{[1+(\alpha\,|\,\psi\,|\,)^n]^m}\\ k_r(\psi)&=\frac{\left\{1-(\alpha\,|\,\psi\,|\,)^{n-1}[1+(\alpha\,|\,\psi\,|\,)^n]^{-m}\right\}^2}{[1+(\alpha\,|\,\psi\,|\,)^n]^{m/2}}\end{aligned}\right\} \tag{7}$$

where θ_s and θ_r are the saturated and residual water contents respectively, and α, n, m are the model parameters with $m=1-1/n$.

2.2.2. Governing Equations of Seepage–Stress Coupling

Considering the coupling interaction between seepage field and stress field, based on Biot's consolidation theory, the stress equilibrium equation is:

$$\sigma_{ij,j}+\gamma_i-\alpha\delta_{ij}p_{,i}=0 \tag{8}$$

Geometric equations and constitutive equations:

$$\left.\begin{aligned}\varepsilon_{ij}&=\tfrac{1}{2}(u_{i,j}+u_{j,i})\\ \sigma_{ij}&=2G\varepsilon_{ij}+\lambda\varepsilon_{kk}\delta_{ij}-\alpha p\delta_{ij}\end{aligned}\right\} \tag{9}$$

where σ_{ij} is the effective stress, u is the displacement, p is the pore water pressure, λ and G are the Lamé constants, α is the Biot coefficient, and γ_i is the component of the specific weight.

Combined with the seepage governing equation, a set of seepage–stress coupling equations under the random field is formed to characterize the mechanical responses such as surrounding rock deformation and lining force induced by tunnel seepage.

2.2.3. Coupled Model of Geo-Ecological Environment Response

Tunnel seepage affects surface vegetation growth, soil physicochemical properties, and karst ecosystems by altering parameters such as groundwater level, soil water content, and pore water pressure, thus constructing a hydrological–ecological coupling response equation:

(a) Groundwater Depth Response Equation:

$$\frac{\partial h_e}{\partial t}=\frac{1}{\mu_s}\left[q_{in}-q_{out}-K(\mathbf{x},\omega)\nabla^2 H\right] \tag{10}$$

where h_e is the groundwater depth, μ_s is the specific yield, and q_{in} and q_{out} are the groundwater recharge and discharge rates, respectively.

(b) Vegetation Coverage Response Equation:

$$\frac{\partial f_v}{\partial t} = \beta_1 f_v(1 - f_v) - \beta_2 \left(\frac{h_e - h_{opt}}{h_{opt}} \right)^2 f_v \tag{11}$$

where f_v is the vegetation coverage, β_1 and β_2 are the growth and stress coefficients, respectively, and h_{opt} is the optimal groundwater depth for vegetation.

(c) Soil Physicochemical Property Response Equation:

$$\frac{\partial C_s}{\partial t} = D_s \nabla^2 C_s - v_s \cdot \nabla C_s + k_s C_s (C_{s0} - C_s) \tag{12}$$

where C_s is the soil nutrient/salt concentration, D_s is the diffusion coefficient, v_s is the soil water transport velocity, k_s is the transformation coefficient, and C_{s0} is the initial concentration.

2.2.4. Coupled Boundary Conditions Under Random Field

Combined with the actual tunnel engineering, the coupled boundary conditions under random field are set as follows:

(a) Hydraulic head boundary: $H(\mathbf{x}, t) = H_0(\mathbf{x}, t), \mathbf{x} \in \Gamma_1$;
(b) Flow rate boundary: $K_{ij}(\mathbf{x}, \omega) \frac{\partial H}{\partial x_j} n_i = q_0(\mathbf{x}, t), \mathbf{x} \in \Gamma_2$;
(c) Displacement boundary: $u_i(\mathbf{x}, t) = u_{i0}(\mathbf{x}, t), \mathbf{x} \in \Gamma_3$;
(d) Ecological boundary: $f_v(\mathbf{x}, t) = f_{v0}(\mathbf{x}, t), \mathbf{x} \in \Gamma_4$.

Through the above equations, the fully coupled characterization of tunnel seepage–mechanical response–geological ecological environment under random field is realized, providing physical constraints for the subsequent prediction model.

The boundary conditions are defined to represent typical tunnel seepage conditions. The hydraulic head boundary corresponds to the far-field groundwater level, while the flow boundary at the tunnel surface represents drainage induced by excavation. The mechanical boundary constrains the outer domain to maintain stability, with deformation concentrated near the tunnel. The ecological variables are initialized according to the initial environmental state and evolve with changes in groundwater conditions. These assumptions are consistent with the two-dimensional tunnel model used in this study.

2.3. PINN-Based Prediction Model for Geo-Ecological Environment Response

2.3.1. Basic Principles of PINN

Physics-informed neural networks (PINNs) are based on fully connected neural networks. They embed physical governing equations, boundary conditions and initial conditions into the loss function as regularization terms, and solve equation derivatives through automatic differentiation, achieving meshless and high-efficiency solution of partial differential equations.

Let the network input be the spatial coordinates $\mathbf{x} = (x, y)$ and time t, and the output be the response field variables $u(\mathbf{x}, t; \theta)$ (hydraulic head, displacement, vegetation coverage, etc.), where θ is the network parameter. The PINN loss function consists of physics loss, boundary loss, initial loss and data loss.

$$Loss(\theta) = Loss_{phys} + \lambda_{bc} Loss_{bc} + \lambda_{ic} Loss_{ic} + \lambda_{data} Loss_{data} \tag{13}$$

where λ_{bc}, λ_{ic} and λ_{data} are the loss weight coefficients.

Definitions of each loss term:

(a) Physics loss: $Loss_{phys} = \frac{1}{N_p}\sum_{i=1}^{N_p}|\mathcal{F}(u(\mathbf{x}_i,t_i;\theta))|^2$, $\mathcal{F}(\cdot)$ is the residual of the physical governing equation;

(b) Boundary loss: $Loss_{bc} = \frac{1}{N_{bc}}\sum_{i=1}^{N_{bc}}|u(\mathbf{x}_i,t_i;\theta) - u_{bc}(\mathbf{x}_i,t_i)|^2$;

(c) Initial loss: $Loss_{ic} = \frac{1}{N_{ic}}\sum_{i=1}^{N_{ic}}|u(\mathbf{x}_i,0;\theta) - u_{ic}(\mathbf{x}_i)|^2$;

(d) Data loss: $Loss_{data} = \frac{1}{N_{data}}\sum_{i=1}^{N_{data}}|u(\mathbf{x}_i,t_i;\theta) - u_{obs}(\mathbf{x}_i,t_i)|^2$.

The loss function is minimized by the Adam optimization algorithm to obtain the response field prediction values satisfying physical laws.

2.3.2. PINN Architecture Fused with Uncertainty

The random vector ξ obtained by discretizing the random field in the previous section is taken as an additional input of PINN to construct a random field–PINN coupling architecture, realizing the fusion of uncertainty and physical constraints; Figure 2 shows the architecture flow chart. The network structure is as follows:

(a) Input layer: spatial coordinates (x, y), time t, and random field random variable ξ;
(b) Hidden layer: 8 fully connected layers with 128 neurons per layer, using the Tanh activation function (to ensure infinite differentiability);
(c) Output layer: multi-field response variables such as hydraulic head H, pore water pressure p, displacement u, groundwater depth h_e, and vegetation coverage f_v;
(d) Loss layer: embedding the random field coupling governing equations, boundary conditions, and initial conditions to construct the uncertainty-aware physics loss function.

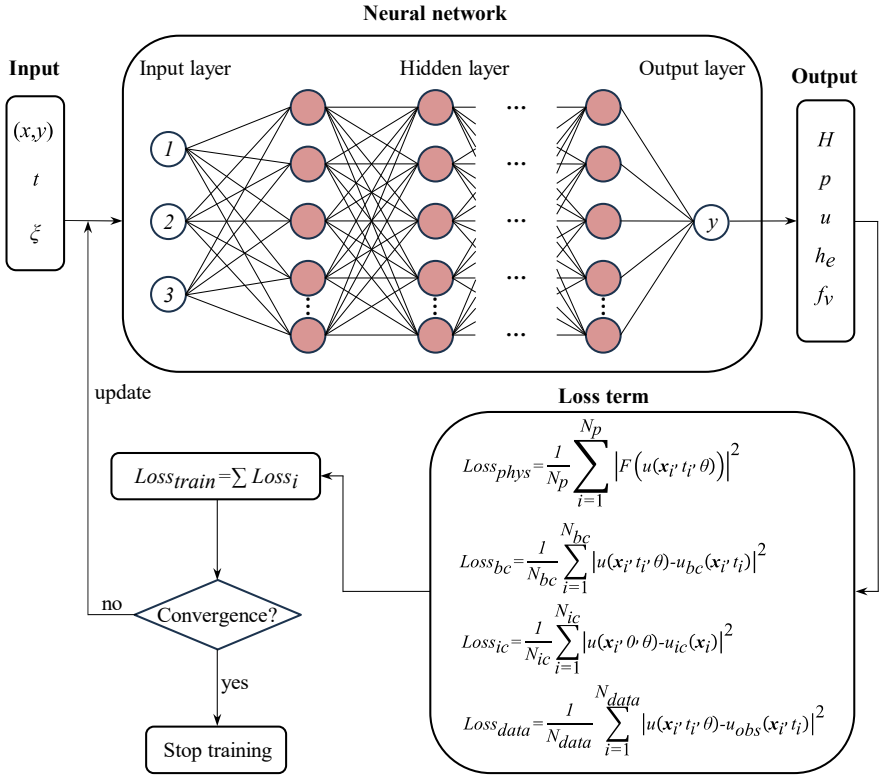


Figure 2. PINN-based framework for geo-ecological environment response.

Physics loss function fused with uncertainty:

$$Loss_{phys}^{U} = \frac{1}{N_p N_\xi} \sum_{i=1}^{N_p} \sum_{j=1}^{N_\xi} |\mathcal{F}(u(\mathbf{x}_i, t_i, \boldsymbol{\xi}_j; \boldsymbol{\theta}))|^2 \quad (14)$$

where N_ξ is the number of random variable samples.

This architecture couples the spatial randomness of the parameter random field with temporal evolution, realizing deterministic prediction and uncertainty quantification of the geo-ecological environment response field, and outputs statistical characteristics such as the mean, variance, and confidence interval of the response field.

2.3.3. Model Training and Validation Process

(a) Input layer: Collect hydrogeological parameters of actual engineering tunnels (permeability coefficient, porosity, correlation length, etc.) to construct a parameter random field; generate training data, including spatial–temporal random variable sampling points, boundary/initial conditions, and field monitoring data; perform data normalization to map input and output data to the interval $[-1, 1]$ to improve training stability.

(b) Network training: Initialize network parameters θ, set learning rate $lr = 10^{-4}$ and number of epochs = 20,000; compute the residual of the governing equation using automatic differentiation and update the loss function; minimize the loss via the Adam optimization algorithm, with an early stopping strategy to prevent overfitting. The PINN model was implemented in Python version 3.14.5 (Python Software Foundation, Wilmington, DE, USA). Data preprocessing, model training, automatic differentiation, and statistical evaluation were all performed in the Python environment.

(c) Model validation: Evaluate prediction accuracy using mean squared error (MSE), coefficient of determination (R^2), and mean absolute error (MAE); verify uncertainty by comparing the predicted statistical characteristics of the response field with simulation results; compare the predicted results with field monitoring data of actual engineering tunnels (water inflow, groundwater level, vegetation coverage) to verify engineering applicability.

For reproducibility, the input variables of the PINN include spatial coordinates, time, and the random variables derived from the K-L expansion, while the outputs correspond to the multi-field responses defined in Section 2.2. The field monitoring dataset used in this study includes groundwater level, tunnel water inflow, and vegetation coverage collected at multiple monitoring points along the tunnel. A total of approximately 180 monitoring samples were used. The monitoring points are distributed along the tunnel and surrounding affected area, with a spatial resolution of approximately 10–20 m, which is consistent with the correlation length used in the random field model. The temporal resolution of the monitoring data is monthly, covering the construction and early operation stages. Before model training, the monitoring data were preprocessed to reduce measurement noise. Abnormal values outside the physically reasonable range were removed, and missing values were interpolated using linear interpolation. All variables were then normalized to the interval $[-1, 1]$ to improve training stability. For validation, the PINN predictions were compared with both numerical simulation results and field monitoring data using statistical indicators (MSE, MAE, and R^2) as well as the consistency of temporal evolution trends, ensuring agreement between simulations and observations. The weighting coefficients in the loss function were determined through sensitivity analysis to balance physical constraints and data fitting, ensuring that the model satisfies the governing equations while effectively incorporating measured information.

3. Results Analysis

3.1. Project Overview and Calculation Parameters

Taking a karst tunnel in Chongqing as a case study, the study area is in a typical carbonate karst region in Southwest China. The strata are mainly composed of limestone and dolomite with interbedded mudstone, and are characterized by well-developed fractures, faults, and strong karstification. These geological features result in highly heterogeneous hydrogeological conditions and the formation of preferential groundwater flow channels. The regional groundwater system is primarily recharged by atmospheric precipitation, with infiltration occurring through fractures and karst conduits. Groundwater runoff is mainly controlled by the karst network and structural features, and discharge typically occurs through springs and low-lying areas, showing significant spatial variability. Based on engineering investigation reports and field monitoring data of the project, the hydrogeological parameters are determined, including a permeability coefficient K = 0.05~0.35 m/d, correlation length λc = 10~20 m, and porosity n = 0.15~0.25. These parameters exhibit clear spatial variability and their statistical characteristics are used to support the construction of the random field in the model. The available monitoring data include groundwater level, tunnel water inflow, and ecological indicators. The surface vegetation is dominated by shrubs and arbor trees.

The calculation model adopts a typical tunnel section with a size of 100 m × 100 m, a tunnel radius of 5.25 m, and a buried depth of 80 m. To balance calculation accuracy and efficiency, the first 20 terms of the K-L expansion are intercepted to realize random field discretization. Five comparative cases are set—Case 1 (low-permeability homogeneous), Case 2 (medium-permeability homogeneous), Case 3 (high-permeability homogeneous), Case 4 (random coupling of multi-parameter random fields), and Case 5 (deterministic mean simulation)— to systematically reveal the regulatory mechanism of parameter spatial variability on the tunnel water seepage–geo-ecological response. To clarify the modeling strategy, the five calculation cases are designed to distinguish the effects of parameter magnitude and spatial variability. The homogeneous cases represent different overall seepage levels under uniform conditions, while the deterministic mean case serves as a reference for averaged parameter behavior. The random-field case is introduced to capture spatial heterogeneity and to evaluate its deviation from the mean-field assumption.

3.2. Random Field Generation Results

The discretization and characterization of the permeability coefficient random field are completed based on the K-L expansion, and the results are shown in Figures 3–5. It can be seen from Figure 3 that the permeability coefficient around the tunnel exhibits significant spatial variability, and the high-permeability zones are concentrated in karst-developed and joint-intensive sections, which are consistent with the revealed geological laws. Figure 4 compares different random field realizations. Under the same meaning, variance and correlation length, there are obvious differences in the local permeability coefficient distribution, which directly reflects the random nature of the hydrogeological parameters of the surrounding rock.

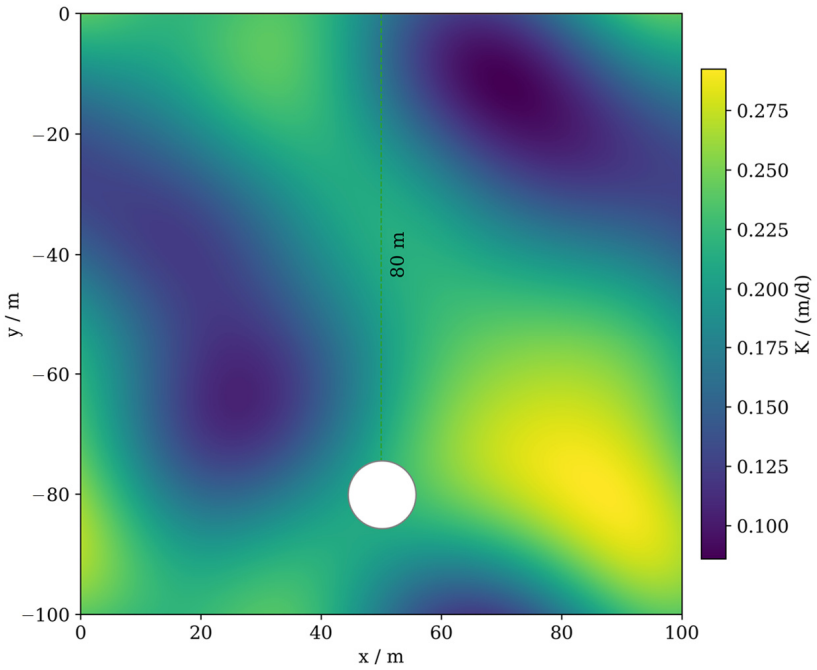


Figure 3. Random field distribution of permeability coefficient around the tunnel.

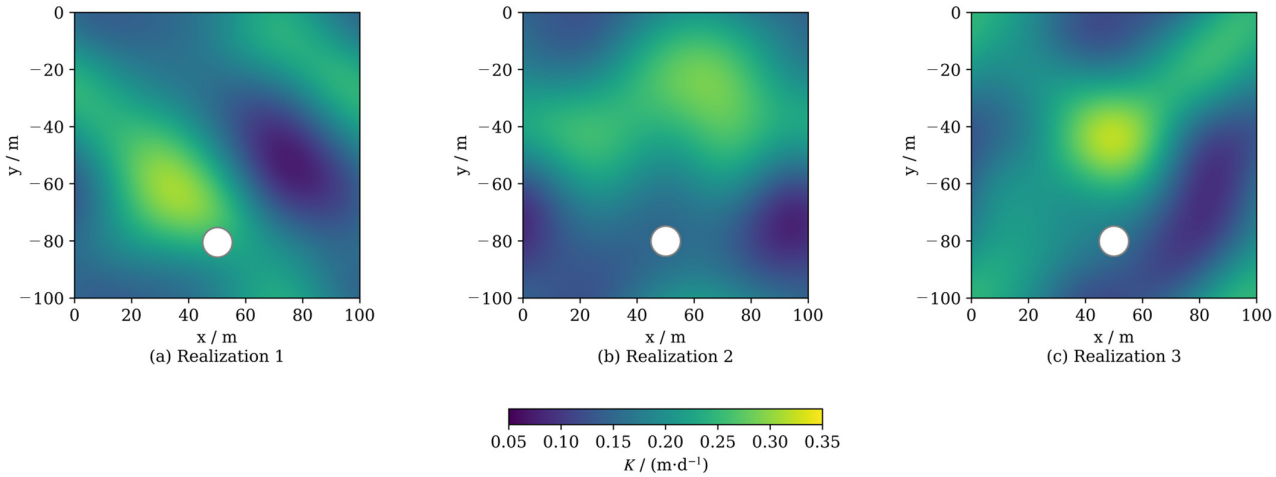


Figure 4. Comparison of permeability coefficient random fields for different realizations.

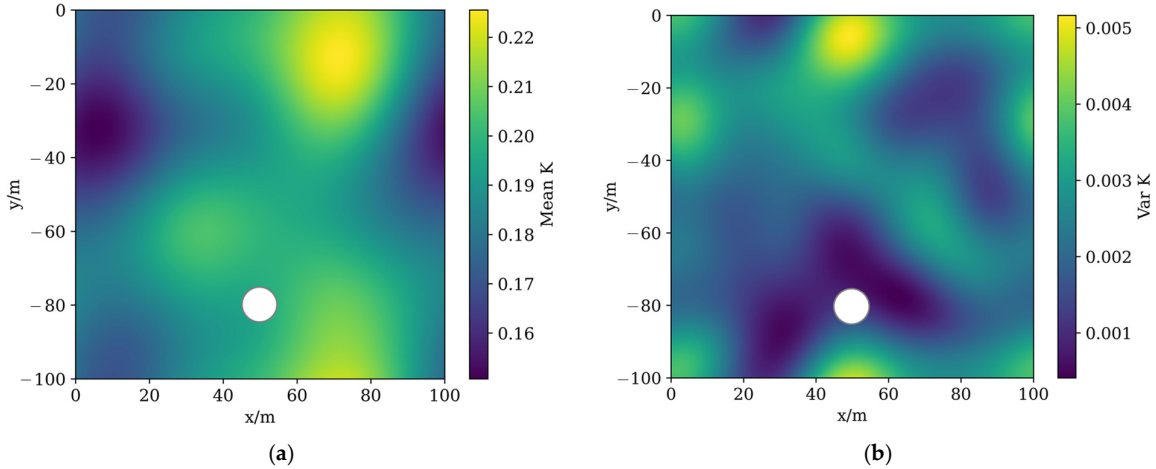
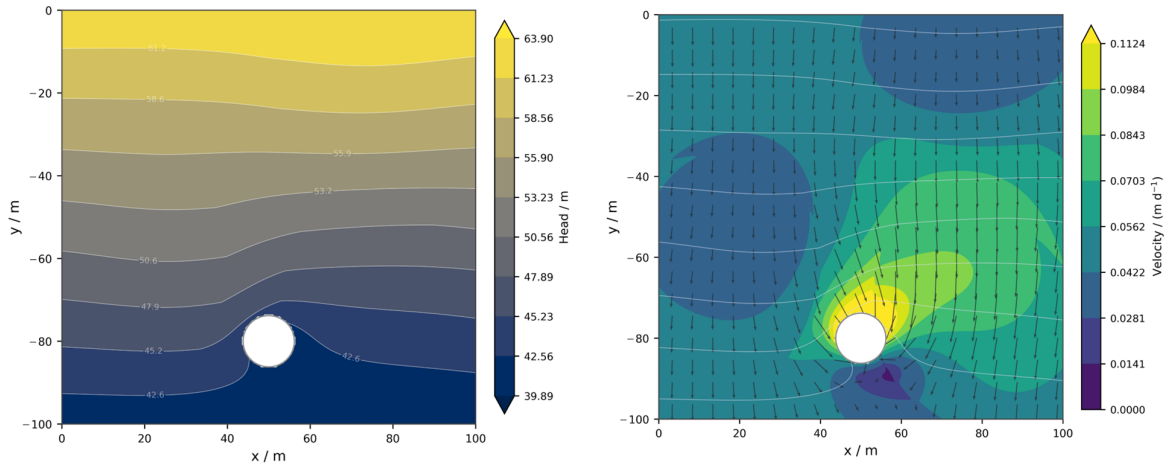


Figure 5. Statistical characteristic distribution of the random field: (**a**) Mean distribution of the random field; (**b**) variance distribution of the random field.

Figure 5 shows the statistical characteristic distribution of the random field, in which the mean field presents a pattern of slow outward transition centered on the tunnel, and the variance field peaks at the tunnel free face and karst-developed areas, indicating that the parameter uncertainty is most prominent in this region. The discretization error of the random field is less than 3%, which meets the accuracy requirements of multi-field coupling calculation and can provide reliable parameter input for the subsequent ecological response analysis under water seepage conditions.

3.3. Response Results of Seepage Field for Tunnel Water Seepage

The evolution of the seepage field caused by tunnel water seepage is the core driving force for changes in the geo-ecological environment. This paper systematically analyzes the hydraulic head distribution, seepage velocity, and water inflow time history, and the results are shown in Figures 6 and 7.



(**a**) (**b**)

Figure 6. Response results of tunnel seepage field: (**a**) Nephogram of hydraulic head distribution; (**b**) seepage velocity vector.

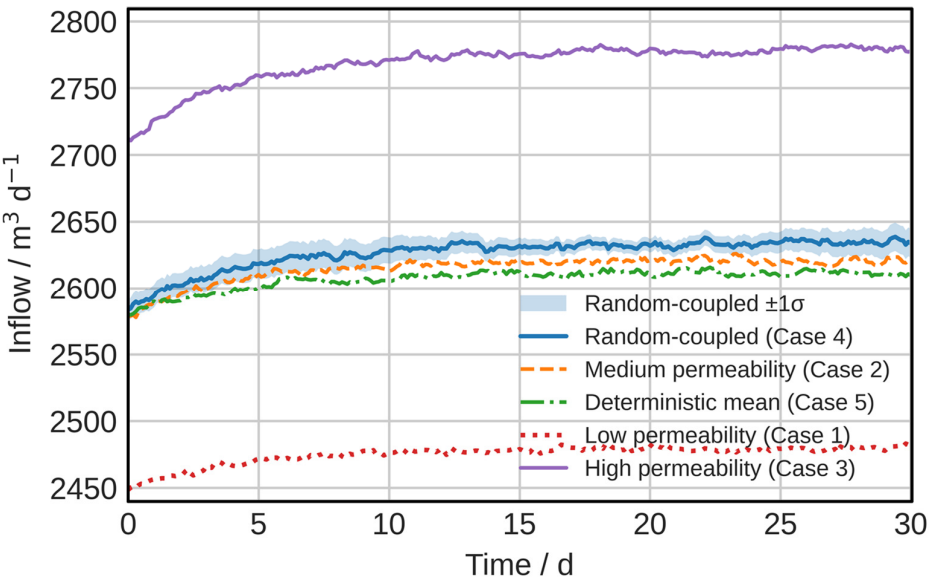


Figure 7. Time–history curves of tunnel water inflow under different cases.

Figure 6a is the nephogram of hydraulic head distribution in the typical tunnel section. Affected by tunnel excavation unloading and seepage convergence, groundwater forms

an obvious drawdown funnel centered on the tunnel, and the hydraulic gradient reaches the maximum near the tunnel contour. The hydraulic head drop in high-permeability zones is significantly larger than that in low-permeability zones, with a wider and more irregular drawdown funnel, reflecting the control effect of parameter spatial variability on the seepage field. Figure 6b is the seepage velocity vector field. The dominant seepage channels are fully coupled with the high-value areas of the permeability coefficient random field. The flow velocity in karst fracture zones is significantly higher than that in intact rock mass sections, and water flows rapidly toward the tunnel free face, forming local concentrated seepage channels, which are highly consistent with the actual tunnel water inflow and dripping positions.

Figure 7 shows the time–history response curves of tunnel water inflow under different cases, all of which exhibit a three-stage evolution law of rapid rise, slow growth, and stabilization. Among them, the high-permeability case (Case 3) has the maximum steady-state water inflow, reaching 2788 m^3/d; the low-permeability case (Case 1) has the minimum steady-state water inflow, at 2485 m^3/d; the random field coupling case (Case 4) has a steady-state water inflow of 2640 m^3/d, which is between the medium-permeability case (Case 2) and high-permeability case (Case 3); the deterministic mean value case (Case 5) has a water inflow of 2616 m^3/d, slightly lower than that of the random field case. The above results indicate that the traditional deterministic mean value model will smooth out the concentrated seepage effect in the high-permeability zone, leading to conservative water inflow prediction, while the random field model can more truly reflect the seepage characteristics of heterogeneous rock masses.

3.4. Geo-Ecological Environment Response Results

Long-term tunnel water seepage alters the groundwater circulation path and distribution state, thereby driving a cascading response in the surface ecosystem. This paper focuses on analyzing three core ecological indicators: groundwater depth, vegetation coverage, and soil physicochemical properties, as shown in Figures 8–10.

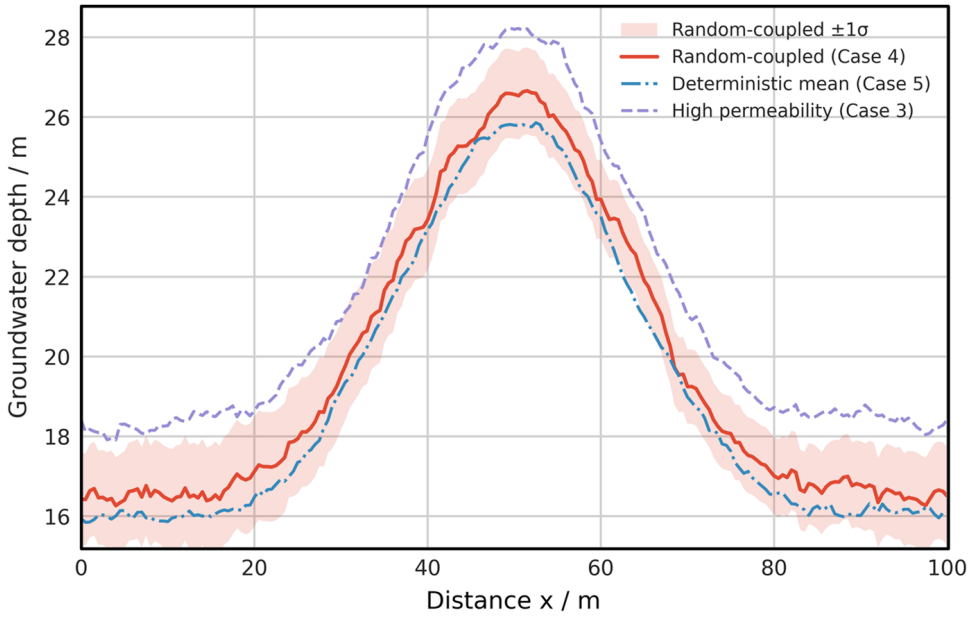


Figure 8. Response curve of groundwater depth.

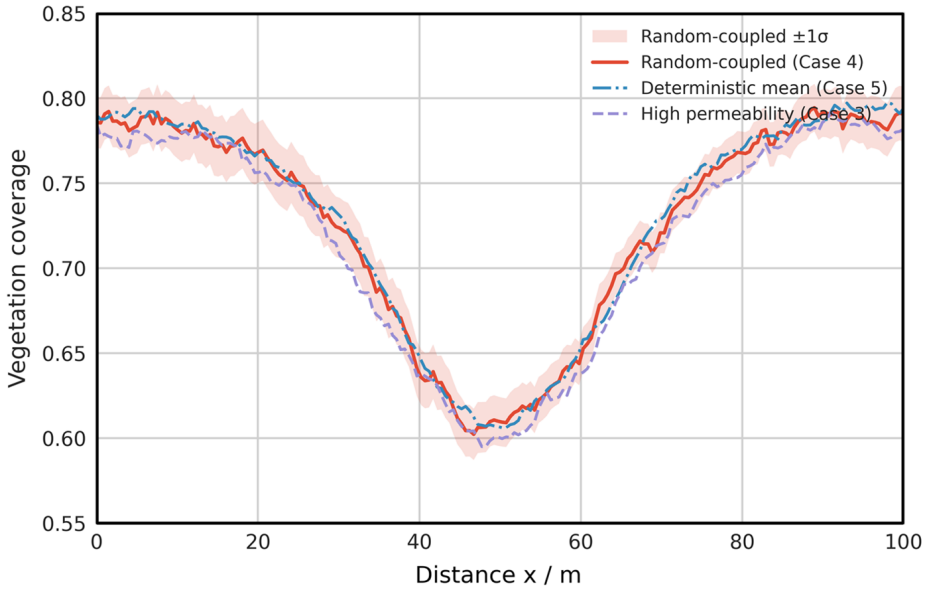


Figure 9. Response curve of vegetation coverage.

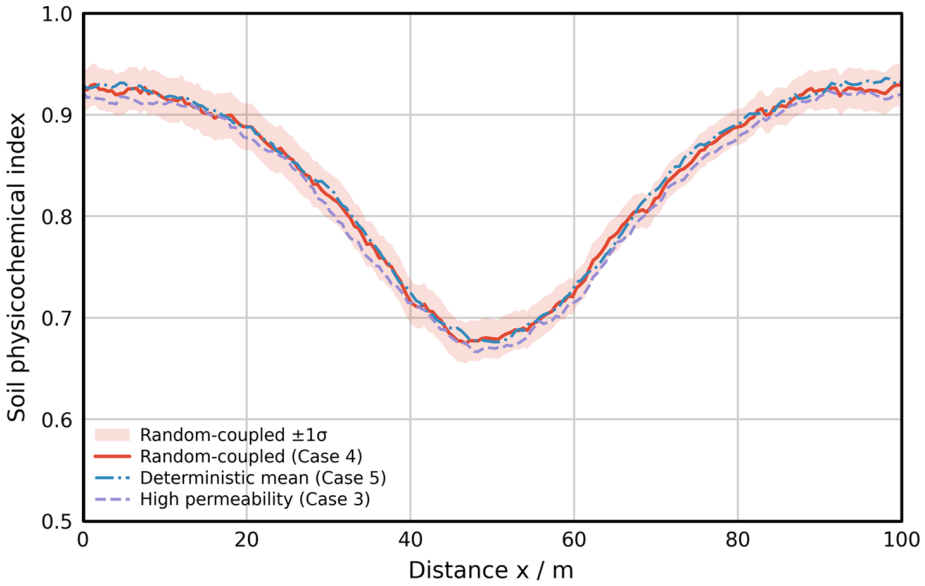


Figure 10. Response curve of soil physicochemical properties.

Figure 8 presents the time-varying curves of groundwater depth under different cases. The continuous extraction of groundwater due to tunnel seepage leads to a persistent decline in groundwater level and a continuous increase in burial depth, which eventually stabilizes. The high-permeability case (Case 3) exhibits the maximum drawdown of 15.6 m and the widest groundwater drainage range; the random field coupling case (Case 4) has a maximum drawdown of 12.4 m, which is higher than the 11.8 m of the deterministic mean case (Case 5). This difference stems from the formation of dominant seepage channels in high-permeability zones within the random field, accelerating groundwater drainage. It indicates that the spatial variability of parameters will significantly exacerbate the magnitude of groundwater decline, and traditional deterministic models will underestimate the risk of groundwater drainage.

Figure 9 shows the response curve of vegetation coverage. Affected by the increase in groundwater depth and soil water stress, vegetation coverage gradually decreases with seepage time and eventually stabilizes. The high-permeability case (Case 3) has the largest reduction in vegetation coverage, reaching 19.4%; the random field coupling case

(Case 4) has a reduction of 14.8%, which is higher than the 13.7% of the deterministic mean case (Case 5).

Figure 10 shows the response curves of soil physicochemical indicators. The decline in groundwater level changes the processes of soil water migration, salt accumulation, and nutrient transformation, resulting in a decrease in soil nutrient concentration and the increase in salinization risk. The high-permeability case (Case 3) shows a reduction of 16.8% in soil indicators; the random field coupling case (Case 4) shows a reduction of 12.2%, which is also higher than the 11.4% of the deterministic mean case (Case 5). The soil response is completely synchronized with groundwater depth and vegetation coverage, forming a "groundwater–soil–vegetation" chain response structure, and the random field makes the whole chain response stronger and spatial differences more significant.

To summarize, considering the random field of hydrogeological parameters significantly amplifies the negative impact of tunnel water seepage on the surface ecosystem, and the traditional deterministic mean model exhibits an obvious underestimation effect on ecological risks.

3.5. PINN Model Prediction Results

Figure 11 shows the training loss convergence curves of the PINN model, including the total loss and sub-losses such as physics loss, boundary loss, initial loss, and data loss. It can be seen that the total loss and sub-losses decrease rapidly at the initial stage of iteration, the descent rate slows down after 5000 iterations and basically converges and stabilizes after 15,000 iterations. This indicates that the model has fully learned the physical laws of seepage–stress ecology coupling under random fields, with strong fitting ability, good stability, and no obvious oscillation or overfitting phenomenon, meeting the prediction requirements. Table 1 shows the statistical indicators of the prediction performance of the PINN model. For the training set, MSE = 6.4×10^{-4}, MAE = 0.0158, R^2 = 0.986; for the validation set, MSE = 8.7×10^{-4}, MAE = 0.0196, R^2 = 0.978, and the coverage rate of the 95% confidence interval reaches 91.1%. The prediction accuracy meets the requirements of engineering applications.

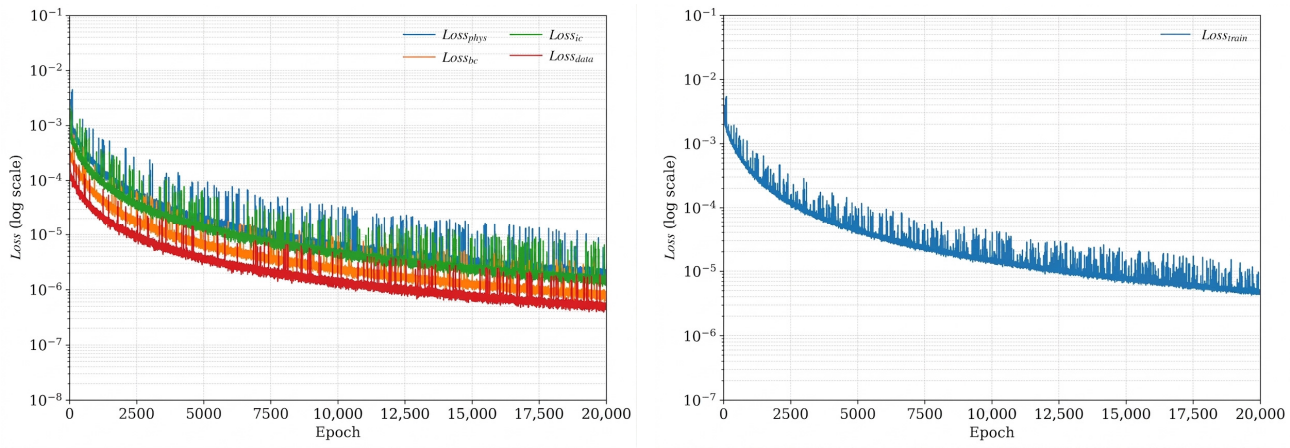
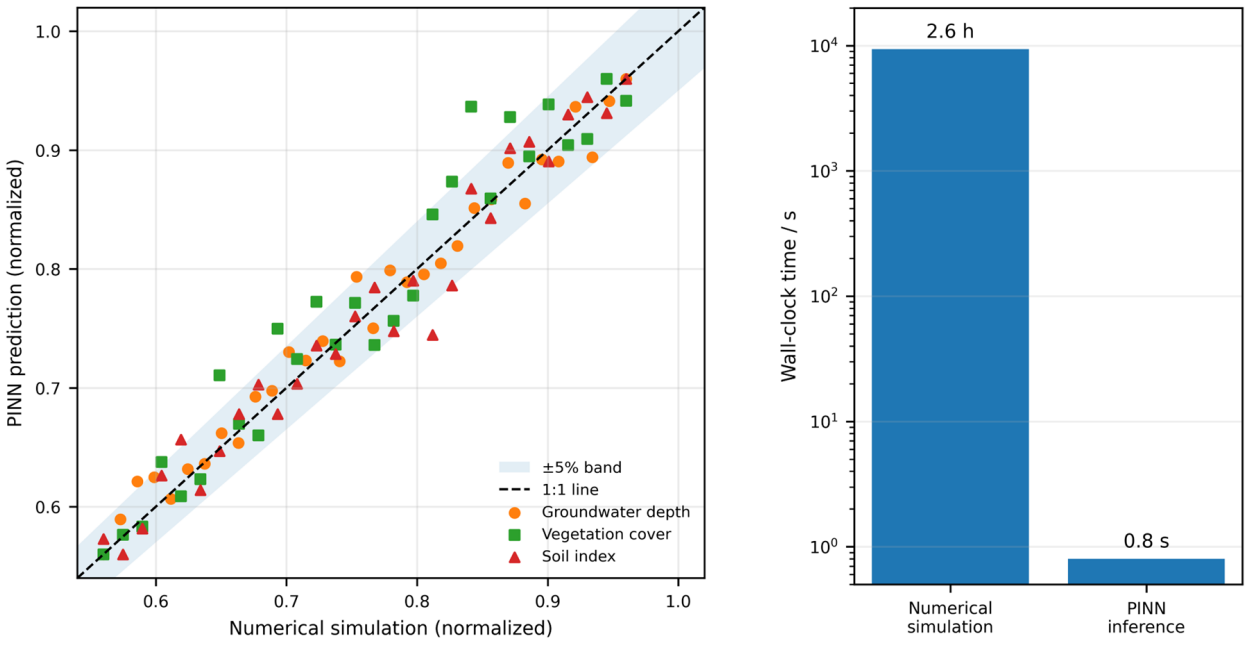


Figure 11. Convergence process of PINN training loss: (**a**) Various loss values; (**b**) total loss value.

Table 1. Statistics of PINN fast prediction performance.

Indicator	Training Set	Validation Set	Description
MSE	6.4×10^{-4}	8.7×10^{-4}	Output targets: groundwater depth, vegetation coverage, soil physicochemical index.
MAE	0.0158	0.0196	Numerical simulation for a single case takes approximately 2.6 h, while PINN inference takes only about 0.8 s
R^2	0.9860	0.9780	The validation set samples generally fall near the 1:1 line and within the ±5% error band.
95% confidence interval coverage rate	92.3%	91.1%	It is suitable for rapid screening and uncertainty quantification of random field cases.

Figure 12a shows the consistency comparison between predicted and true values. All sample points are closely distributed near the 1:1 reference line and fall entirely within the ±5% error band, indicating that the model has high reliability in predicting groundwater depth, vegetation coverage, and soil physicochemical index. Figure 12b presents the comparison of computational efficiency. The traditional numerical simulation takes approximately 2.6 h to solve a single case, whereas the PINN model in this study only requires 0.8 s for single-case inference, improving computational efficiency by about 11,700 times and realizing rapid prediction of multi-field responses under random fields.



(**a**) (**b**)

Figure 12. Prediction consistency and fast prediction capability of PINN: (**a**) Prediction consistency; (**b**) computational efficiency.

The coupled random field and PINN model can directly output statistical characteristics such as the mean, variance, and 95% confidence interval of the response field, enabling uncertainty quantification analysis. The prediction results show that the uncertainty is the greatest around the tunnel and in karst-developed areas, which is consistent with the variance distribution of the random field. This indicates that the model can effectively capture the response fluctuations caused by spatial parameter variability, providing a quantitative basis for engineering risk assessment.

3.6. Multi-Case Comparative Analysis

Table 2 and Figure 13 systematically compare key indicators under five working conditions, including steady-state water inflow, maximum drawdown, maximum lining displacement, vegetation coverage reduction, and soil index reduction. The results reveal clear engineering laws: Higher permeability leads to greater tunnel water inflow, groundwater drawdown, lining deformation, and ecological index reduction, which conforms to the basic mechanical and ecological laws of karst tunnel water seepage. All response indicators of the random field coupling case (Case 4) are higher than those of the deterministic mean case (Case 5), confirming that spatial variability of parameters significantly strengthens the mechanical effect of seepage and negative ecological impact. Maximum lining displacement is significantly positively correlated with ecological reduction, indicating that surrounding rock deformation and groundwater drainage jointly drive ecological degradation, and the random field further highlights this multi-field synergistic effect. The response of the random field case falls between that of medium-permeability and high-permeability homogeneous cases. This behavior reflects the combined influence of spatial averaging and local heterogeneity. Although high-permeability zones in the random field can form preferential flow channels and locally enhance seepage intensity, their spatial extent is limited. The overall system response is still largely governed by the background permeability level, which is close to the medium-permeability condition. In addition, the development of high-permeability flow paths is constrained by boundary conditions and hydraulic gradients, preventing their full contribution from dominating the global response. Therefore, the random field response represents a nonlinear integration of the average field effect and localized high-permeability amplification, rather than a simple dominance of extreme values. The results under random field conditions should not be interpreted as a simple compromise between medium and high permeability cases, but as the outcome of the interaction between spatial variability and flow regulation mechanisms.

Table 2. Comparison of key response indicators under multiple cases.

Case	Steady-State Water Inflow/(m^3/d)	Maximum Drawdown/m	Lining Displacement/mm	Vegetation Coverage Reduction/%	Soil Index Reduction/%
Case 1: Low permeability	2485	7.8	2.1	8.1	6.4
Case 2: Medium permeability	2622	10.9	2.8	12.6	10.3
Case 3: High permeability	2788	15.6	3.9	19.4	16.8
Case 4: Random field coupling	2640	12.4	3.1	14.8	12.2
Case 5: Deterministic comparison	2616	11.8	2.9	13.7	11.4

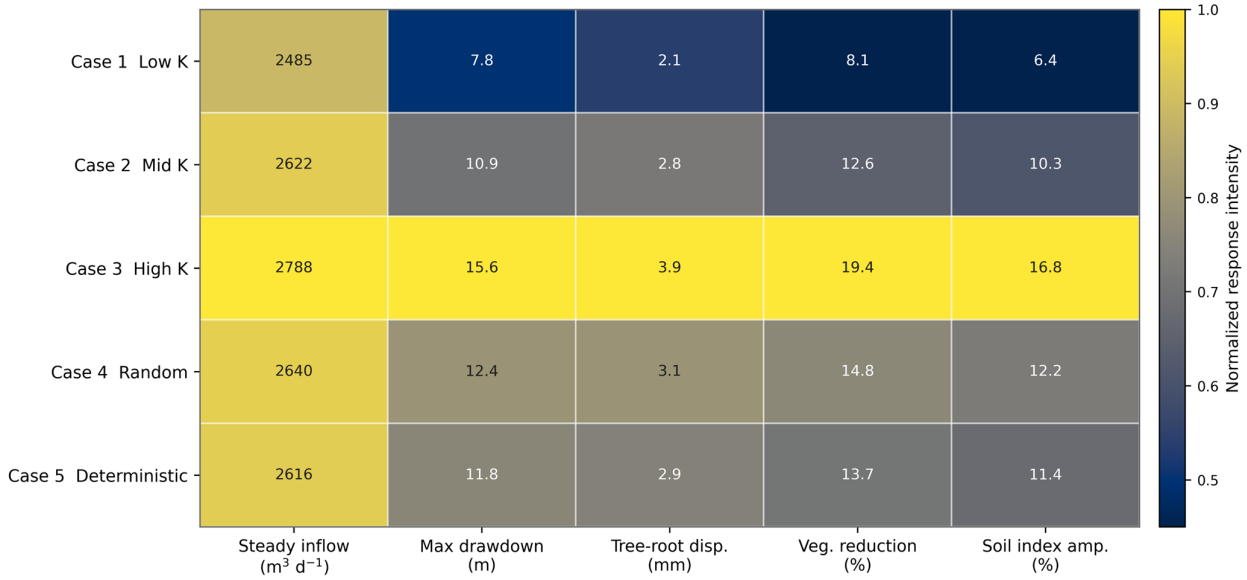


Figure 13. Comparison diagram of multi-case responses.

4. Discussion

4.1. Influence Mechanism of Random Field on Tunnel Seepage–Geological–Ecological Response

Previous studies have demonstrated that geological heterogeneity plays a key role in controlling seepage processes, whereas deterministic approaches tend to smooth spatial variability. In this study, the random-field model captures high-permeability zones associated with karst fissures and jointed structures, forming preferential flow paths that significantly enhance local seepage velocity and water inflow. As a result, the groundwater depression cone shifts toward these regions, leading to heterogeneous groundwater drawdown. To provide a more intuitive comparison of the coupled hydro–mechanical responses under different permeability scenarios, Figure 14 presents the variation in maximum groundwater drawdown and lining displacement across the five cases. It can be observed that the response under the random field condition (Case 4) lies between the medium- and high-permeability cases, while remaining closer to the medium-permeability level.

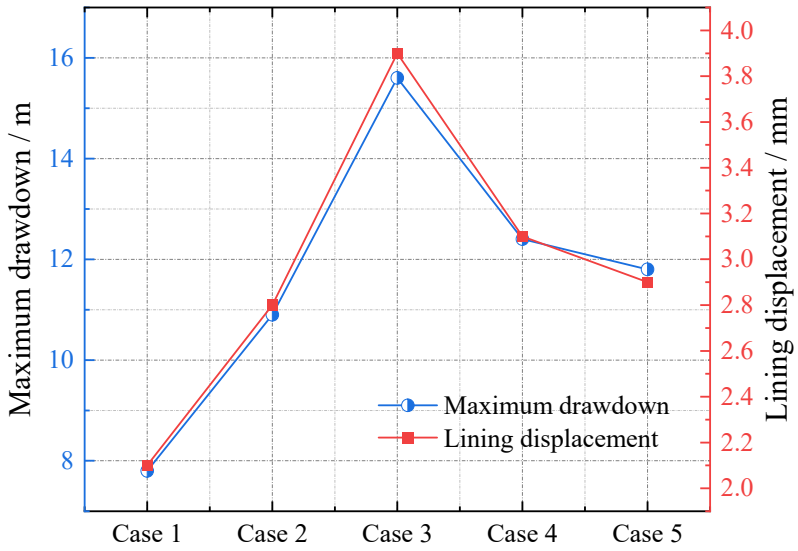


Figure 14. Comparison of groundwater drawdown and lining displacement under different permeability scenarios.

Spatial variability is further transmitted and amplified through the seepage–stress–ecology coupling process, producing localized extreme responses. The ranges of groundwater depth, vegetation coverage, and soil quality increase with the variability of parameters. In contrast, deterministic models assume spatially averaged properties, which suppress local extremes and tend to underestimate seepage intensity and associated ecological risks. Therefore, the stochastic approach provides a more realistic representation of both the magnitude and spatial distribution of multi-field responses. The trends shown in Figure 14 are consistent with the overall results summarized in Table 2, indicating that the random field leads to enhanced but spatially constrained responses rather than uniform amplification. In addition, the joint random field of permeability, porosity, and specific storage enhances the coupling among seepage, stress, and ecological fields. Changes in seepage conditions induce stress redistribution, which in turn affects permeability, forming a feedback mechanism that intensifies ecological degradation. Compared with single-parameter randomness, multi-parameter random fields better reflect the complexity of real engineering systems.

4.2. Advantages and Applicability of the Coupled PINN Model

The proposed PINN framework incorporates governing equations into the loss function, ensuring that predictions satisfy physical conservation laws and remain interpretable. By introducing random variables derived from the K-L expansion, the model effectively integrates spatial variability into the learning process and enables direct uncertainty quantification.

Compared with traditional numerical methods, the proposed approach significantly improves computational efficiency, reducing simulation time from hours to seconds. This advantage makes it particularly suitable for multi-scenario analysis, parameter sensitivity studies, and rapid assessment in engineering applications. In addition, the model can be integrated with monitoring systems to support real-time prediction and decision-making.

4.3. Engineering Application Value and Limitations

It solves the problem that traditional deterministic models underestimate the ecological impact of tunnel seepage, providing a scientific basis for ecological protection, vegetation restoration, and groundwater control in tunnel site areas. It can rapidly complete the screening of many random field cases, optimize the lining structure, drainage system, and grouting scope, and reduce cost and construction period. In sudden events such as water and mud inrush, it can provide the seepage range and ecological impact degree in seconds to support rapid disposal. It can predict the changes in groundwater, vegetation, and soil for several months to years, offering a reference for long-term ecological monitoring and restoration.

However, the model also has limitations. This study adopts a second-order stationary random field and exponential covariance function; for extremely heterogeneous and non-stationary strata, the covariance model needs to be improved, or non-stationary random fields should be adopted. The two-dimensional model cannot fully restore the three-dimensional seepage paths and differences in ecological responses. Three-dimensional expansion will further improve accuracy but correspondingly increase computational cost. The ecological response adopts simplified empirical equations without considering complex factors such as plant species differences, seasonal variations, and human activities. The model accuracy relies on geological survey and monitoring data, and the generalization ability will be affected when data are insufficient.

4.4. Future Research Directions

Construct a three-dimensional K-L random field and 3D PINN architecture to achieve high-precision prediction of seepage–mechanical–ecological responses in real spatial mor-

phology. Combined with long-term monitoring data, establish a temporal PINN model for online parameter updating and dynamic prediction. Integrate the prediction model with optimization algorithms to realize multi-objective collaborative optimization of tunnel structural safety, water inflow control, and ecological protection. Combine Monte Carlo simulation with PINN to conduct probabilistic assessment of low-probability, high-risk water inrush and ecological degradation events.

5. Conclusions

This study develops a stochastic hydro–mechanical–ecological coupled framework by integrating random field theory with PINN to investigate tunnel-induced seepage and its environmental impacts under spatially heterogeneous conditions. The main conclusions are as follows:

(1) Spatial variability plays a dominant role in controlling seepage behavior. Compared with deterministic models, the random-field case consistently produces higher seepage intensity and stronger spatial heterogeneity of groundwater drawdown, with localized responses significantly exceeding the mean-field predictions.
(2) Tunnel-induced seepage leads to a coupled response of groundwater, soil, and vegetation. Groundwater depletion is accompanied by coordinated changes in soil properties and vegetation coverage, showing a clear propagation from subsurface hydrological variation to surface ecological response.
(3) Parameter uncertainty amplifies eco-environmental impacts. Under stochastic conditions, the predicted groundwater drawdown, vegetation reduction, and soil deterioration are consistently greater than those obtained from deterministic simulations, indicating a systematic underestimation of risk when spatial variability is neglected.
(4) The proposed stochastic PINN framework provides accurate and efficient prediction of multi-field responses. The model achieves high prediction accuracy while maintaining computational efficiency, and captures the statistical characteristics of system responses under uncertainty.

The proposed framework can support more reliable assessment of tunnel seepage and its environmental impacts in heterogeneous formations, and provides a reference for similar subsurface engineering problems under spatial variability conditions. Despite these contributions, some limitations should be noted. The present study is based on a two-dimensional framework and assumes stationary random fields, which may limit its applicability to highly complex geological conditions. Future research should extend the model to three-dimensional and non-stationary scenarios, as well as incorporate time-dependent processes and field monitoring data to further improve prediction accuracy and practical applicability.

Author Contributions: Conceptualization, B.W. and Z.L.; Methodology, B.W. and Z.L.; Software, X.P.; Validation, X.P.; Formal analysis, B.W., X.P. and Z.L.; Investigation, B.W. and X.P.; Resources, B.W.; Writing—original draft, B.W., X.P. and Z.L.; Writing—review and editing, B.W. and Z.L.; Visualization, Z.L.; Supervision, Z.L. All authors have read and agreed to the published version of the manuscript.

Funding: This research was funded by China Railway Group Corporation Limited, under the project "Research on Intelligent Construction and Information Technology for the Sichuan-Tibet Railway", grant number CZ-KEY-03. The funder was not involved in the study design, data collection, analysis, interpretation of data, the writing of this article, or the decision to submit it for publication.

Data Availability Statement: The data presented in this study are available in the article.

Acknowledgments: The authors gratefully acknowledge the financial support provided by China Railway Group Corporation Limited.

Conflicts of Interest: Author Buyun Wang was employed by the company Anhui Digital Intelligence Construction Research Institute Co., Ltd. The authors declare that this study received funding from China Railway Group Corporation Limited. The funder was not involved in the study design, collection, analysis, interpretation of data, the writing of this article or the decision to submit it for publication.

References

1. Liu, Z.; Gu, X.; Hong, R. Fire protection and evacuation analysis in underground interchange tunnels by integrating BIM and numerical simulation. *Fire* **2023**, *6*, 139. [CrossRef]
2. Xu, H.; Li, X.; Gokdemir, C. Modeling and assessing the impact of tunnel drainage on terrestrial vegetation. *Tunn. Undergr. Space Technol.* **2021**, *116*, 104097. [CrossRef]
3. Gokdemir, C.; Rubin, Y.; Li, X.; Xu, H. A vulnerability assessment method to evaluate the impact of tunnel drainage on terrestrial vegetation under various atmospheric and climatic conditions. *Adv. Water Resour.* **2021**, *147*, 103796. [CrossRef]
4. Gokdemir, C.; Rui, Y.; Rubin, Y.; Li, X. A framework for assessing tunnel drainage-induced impact on terrestrial vegetation. *Tunn. Undergr. Space Technol.* **2023**, *132*, 104917. [CrossRef]
5. Liu, Z.; Gu, X.; Kwan, M.-P.; Cui, B. Integrated ultrasonic testing and numerical simulation for damage detection in steel bridge deck pavements. *Eng. Struct.* **2026**, *355*, 122421. [CrossRef]
6. Zheng, X.; Yang, Z.; Wang, S.; Chen, Y.-F.; Hu, R.; Zhao, X.-J.; Wu, X.-L.; Yang, X.-L. Evaluation of hydrogeological impact of tunnel engineering in a karst aquifer by coupled discrete-continuum numerical simulations. *J. Hydrol.* **2021**, *597*, 125765. [CrossRef]
7. Lv, Y.; Jiang, J.; Chen, L.; Hu, W.; Jiang, Y. Elaborate simulation and predication of the tunnel drainage effect on karst groundwater field and discharge based on Visual MODFLOW. *J. Hydrol.* **2022**, *612*, 128023. [CrossRef]
8. Liu, J.; Li, X. Analytical solution for estimating groundwater inflow into lined tunnels considering waterproofing and drainage systems. *Bull. Eng. Geol. Environ.* **2021**, *80*, 6827–6839. [CrossRef]
9. Zhang, W.; Liu, M.; Bian, K.; Cong, P.-T.; Yuan, W.-H. Modelling the hydro-mechanical behaviour of high-pressure tunnel with emphasis on the interaction between lining and rock mass. *Comput. Geotech.* **2021**, *139*, 104382. [CrossRef]
10. Song, F.; Rodriguez-Dono, A.; Olivella, S. Hydro-mechanical modelling and analysis of multi-stage tunnel excavations using a smoothed excavation method. *Comput. Geotech.* **2021**, *135*, 104150. [CrossRef]
11. Wang, C.; Liu, X.; Song, D.; Wang, E.; Yan, G.; Zhou, R. Three-dimensional hydro-mechanical coupling numerical simulation of shield-driven cross-river twin tunnels: A case study. *Undergr. Space* **2024**, *16*, 106–125. [CrossRef]
12. Zhang, W.; Han, L.; Gu, X.; Wang, L.; Chen, F.; Liu, H. Tunneling and deep excavations in spatially variable soil and rock masses: A short review. *Undergr. Space* **2022**, *7*, 380–407. [CrossRef]
13. Li, T.; Gong, W.; Tang, H. Three-dimensional stochastic geological modeling for probabilistic stability analysis of a circular tunnel face. *Tunn. Undergr. Space Technol.* **2021**, *118*, 104190. [CrossRef]
14. Xie, P.; Luo, H.; Chen, K.; Yang, Z. Random field-based tunneling information modeling framework for probabilistic safety assessment of shield tunnels. *J. Civ. Eng. Manag.* **2023**, *29*, 741–756. [CrossRef]
15. Li, T.; Pan, Q.; Shen, Z.; Gong, W. Probabilistic stability analysis of a tunnel face in spatially random hoek–brown rock masses with a multi-tangent method. *Rock Mech. Rock Eng.* **2022**, *55*, 3545–3561. [CrossRef]
16. Guayacán-Carrillo, L.-M.; Sulem, J.; Ghabezloo, S. Main insights from 2D/3D poroelastic analysis of tunnel excavation in low permeability anisotropic ground. *Comput. Geotech.* **2021**, *130*, 103935. [CrossRef]
17. Dall'Alba, V.; Neven, A.; de Rooij, R.; Filipponi, M.; Renard, P. Probabilistic estimation of tunnel inflow from a karstic conduit network. *Eng. Geol.* **2023**, *312*, 106950. [CrossRef]
18. Zhou, J.; Zhang, Y.; Li, C.; Yong, W.; Qiu, Y.; Du, K.; Wang, S. Enhancing the performance of tunnel water inflow prediction using random forest optimized by grey wolf optimizer. *Earth Sci. Inform.* **2023**, *16*, 2405–2420. [CrossRef]
19. Bai, Y.; Wu, Z.; Huang, T.; Peng, D. A dynamic modeling approach to predict water inflow during karst tunnel excavation. *Water* **2022**, *14*, 2380. [CrossRef]
20. Chen, Z.; Zhang, H.; Shen, Q.; Chen, Z.; Wang, K.; Chen, C. Groundwater flow impact in complex karst regions considering tunnel construction conditions: A case study of the new construction project at xls tunnel. *Water* **2025**, *17*, 2383. [CrossRef]
21. Glanville, K.; Sheldon, F.; Butler, D.; Capon, S. Effects and significance of groundwater for vegetation: A systematic review. *Sci. Total Environ.* **2023**, *875*, 162577. [CrossRef]
22. Hernandez, J.O. Ecophysiological effects of groundwater drawdown on phreatophytes: Research trends during the last three decades. *Land* **2022**, *11*, 2061. [CrossRef]
23. Song, G.; Huang, J.-t.; Ning, B.-h.; Wang, J.-w.; Zeng, L. Effects of groundwater level on vegetation in the arid area of western China. *China Geol.* **2021**, *4*, 527–535. [CrossRef]

24. Yin, L.-h.; Xu, D.-d.; Jia, W.-h.; Zhang, X.-x.; Zhang, J. Responses of phreatophyte transpiration to falling water table in hyper-arid and arid regions, Northwest China. *China Geol.* **2021**, *4*, 410–420. [CrossRef]
25. Qiu, Y.; Wang, D.; Yu, X.; Jia, G.; Li, H. Effects of groundwater table decline on vegetation in groundwater-dependent ecosystems. *Forests* **2023**, *14*, 2326. [CrossRef]
26. Cui, G.; Liu, Y.; Li, X.; Wang, S.; Qu, X.; Wang, L.; Tong, S.; Zhang, M.; Li, X.; Zhang, W. Impacts of groundwater storage variability on soil salinization in a semi-arid agricultural plain. *Geoderma* **2025**, *454*, 117162. [CrossRef]
27. Wu, H.; Bai, J.; Li, J.; Liu, R.; Zhao, J.; Ma, X. The relationships between vegetation changes and groundwater table depths for woody plants in the sangong river basin, northwest china. *Remote Sens.* **2025**, *17*, 937. [CrossRef]
28. Liu, Z.; Yeoh, J.K.; Gu, X.; Dong, Q.; Chen, Y.; Wu, W.; Wang, L.; Wang, D. Automatic pixel-level detection of vertical cracks in asphalt pavement based on GPR investigation and improved mask R-CNN. *Autom. Constr.* **2023**, *146*, 104689. [CrossRef]
29. Secci, D.; Godoy, V.A.; Gómez-Hernández, J.J. Physics-informed neural networks for solving transient unconfined groundwater flow. *Comput. Geosci.* **2024**, *182*, 105494. [CrossRef]
30. Shadab, M.A.; Luo, D.; Hiatt, E.; Shen, Y.; Hesse, M.A. Investigating steady unconfined groundwater flow using physics informed neural networks. *Adv. Water Resour.* **2023**, *177*, 104445. [CrossRef]
31. Ali, A.S.A.; Jazaei, F.; Clement, T.P.; Waldron, B. Physics-informed neural networks in groundwater flow modeling: Advantages and future directions. *Groundw. Sustain. Dev.* **2024**, *25*, 101172. [CrossRef]
32. Cui, B.; Wang, H. Coupled prediction of viscoelastic properties of asphalt mixtures using a multi-task physics-constrained neural network. *Adv. Eng. Inform.* **2026**, *72*, 104437. [CrossRef]
33. Cui, B.; Wang, H. Compatibility analysis of waste polymer recycling in asphalt binder using molecular descriptor and graph neural network. *Resour. Conserv. Recycl.* **2025**, *212*, 107950. [CrossRef]
34. Lei, K.; Cui, B.; Zhang, M.; Mao, R.; Du, Y.; Gu, X.; Liu, Z. Intelligent prediction of pavement structural degradation using a multimodel ensemble learning approach. *Struct. Control Health Monit.* **2026**, *2026*, 6132295. [CrossRef]
35. Cui, B.; Wang, H. Intelligent design of low-carbon asphalt mixtures with enhanced cracking and rutting resistance. *Sustain. Mater. Technol.* **2026**, *48*, e02019. [CrossRef]
36. Cui, B.; Wang, H. Optimization of risk-based and cost-minimized maintenance strategy for corroded pipeline using reinforcement learning. *Reliab. Eng. Syst. Saf.* **2026**, *276*, 112929. [CrossRef]
37. Cui, B.; Wang, H. Predicting asphalt pavement deterioration under climate change uncertainty using bayesian neural network. *IEEE Trans. Intell. Transp. Syst.* **2025**, *26*, 785–797. [CrossRef]

Disclaimer/Publisher's Note: The statements, opinions and data contained in all publications are solely those of the individual author(s) and contributor(s) and not of MDPI and/or the editor(s). MDPI and/or the editor(s) disclaim responsibility for any injury to people or property resulting from any ideas, methods, instructions or products referred to in the content.